Chinese Journal of Oceanology and Limnology
Vol. 33 No. 2, P. 534-544, 2015
http://dx.doi.org/10.1007/s00343-015-4044-7

Why does the IOD-ENSO teleconnection disappear in some decades?*

XU Tengfei (徐腾飞)[1, 2, 4], YUAN Dongliang (袁东亮)[1, 3, **]

[1] *Institute of Oceanology, Chinese Academy of Sciences, Qingdao 266071, China*
[2] *University of Chinese Academy of Sciences, Beijing 100049, China*
[3] *Qingdao Collaborative Innovation Center of Marine Science and Technology, Qingdao 266003, China*
[4] *First Institute of Oceanography, State Oceanic Administration, Qingdao 266061, China*

Received Feb. 20, 2014; accepted in principle Mar. 26, 2014; accepted for publication Jul. 16, 2014

Abstract Lag correlations between sea surface temperature anomalies (SSTA) in the southeastern tropical Indian Ocean (STIO) in fall and Niño 3.4 SSTA in the eastern equatorial Pacific in the following fall are subjected to decadal variation, with positive correlations during some decades and negative correlations during others. Negative correlations are smaller and of shorter duration than positive correlations. Variations in lag correlations suggest that the use of the Indian Ocean Dipole (IOD) as a predictor of the El Niño-Southern Oscillation (ENSO) at a lead time of one year is not effective during some decades. In this study, lag correlations between IOD and ENSO anomalies were analyzed to investigate why the IOD-ENSO teleconnection disappears during decades with negative correlations. Anomalies induced by the IOD in the equatorial Pacific Ocean during decades with negative correlations are still present, but at a greater depth than in decades with positive correlations, resulting in a lack of response to oceanic channel dynamics in the cold tongue SSTA. Lag correlations between oceanic anomalies in the west Pacific warm pool in fall and the equatorial Pacific cold tongue with a one-year time lag are significantly positive during decades with negative correlations. These results suggest that oceanic channel dynamics are overwhelmed by ocean-atmosphere coupling over the equatorial Pacific Ocean during decades with negative correlations. Therefore, the Indonesian throughflow is not effective as a link between IOD signals and the equatorial Pacific ENSO.

Keyword: Indian Ocean Dipole (IOD); El Niño-Southern Oscillation (ENSO); oceanic channel; teleconnection

1 INTRODUCTION

The El Niño-Southern Oscillation (ENSO) is the strongest ocean-atmosphere coupled mode on interannual time scales in the tropical Pacific Ocean. The Indian Ocean Dipole (IOD) is a zonal dipole mode that refers to anomalous cooling in the southeastern tropical Indian Ocean (STIO) and associated anomalous warming in the central and western equatorial Indian Ocean (Saji et al., 1999; Webster et al., 1999). A numbers of studies have suggested that ENSO events have significant impacts on Indian Ocean variability (Klein et al., 1999; Alexander et al., 2002; Lau and Nath, 2003; Cai et al., 2005; Behera et al., 2006; Du et al., 2009). Studies have also suggested that IOD events can affect tropical Pacific sea surface temperature anomalies (SSTA) (Wu and Kirtman, 2004; Annamalai et al., 2005; Xie et al., 2009; Luo et al., 2010; Okomura and Deser, 2010). The mechanisms of IOD forcing on the equatorial Pacific have been attributed to the atmospheric bridge process through the Walker circulation (Ohba et al., 2010; Kug and Ham, 2012; Santoso et al., 2012), and/or to the oceanic channel dynamics through the Indonesian throughflow (ITF) (Yuan et al., 2011, 2013).

Recent studies have suggested that the IOD index

* Supported by the National Basic Research Program of China (973 Program) (Nos. 2012CB956000, 2011CB403502), the National Natural Science Foundation of China (No. 41176019), the China Meteorological Administration (No. GYHY201306018), and the Strategic Priority Program of Chinese Academy of Sciences (No. XDA11010301)
** Corresponding author: dyuan@qdio.ac.cn

could provide improved prediction of the ENSO beyond the spring predictability barrier (Dominiak and Terray, 2005; Izumo et al., 2010, 2013; Yuan et al., 2013). The dynamics responsible for the enhanced predictability have been attributed to the atmospheric bridge (Izumo et al., 2010). Increased convection in the eastern Indian Ocean induces a speed-up of the Walker circulation to generate easterly wind anomalies over the Pacific during the boreal fall of negative IOD periods. The ensuing advective-reflective processes are responsible for a change in the ENSO cycle in the following year. Consequently, a positive IOD often precedes La Niña, whereas a negative IOD precedes El Niño (Izumo et al., 2010).

Based on controlled numerical experiments, Yuan et al. (2011) argued that IOD-forced ITF anomalies enhance the transport of warm water from the upper equatorial Pacific Ocean to the Indian Ocean. The enhanced transport leads to thermocline elevations that generate an upwelling Kelvin wave, which propagates to the eastern equatorial Pacific Ocean favoring anomalous cooling in the Pacific cold tongue with a one-year time lag. This oceanic channel dynamic has been supported by lag correlation analysis of observational data (Yuan et al., 2013). The results have shown significant correlations between STIO SSTA or sea surface height anomalies (SSHA) in fall and SSTA, SSHA, and subsurface temperature anomalies in the central and eastern equatorial Pacific Ocean with a one-year time lag. Conversely, lag correlations between surface zonal wind anomalies (SZWA) in the far western equatorial Pacific in fall and SZWA, SSTA, and SSHA with a one-year time lag are insignificant. Therefore, oceanic channel dynamics, rather than atmospheric bridge processes, are the dominant mechanism for the enhanced predictability of the IOD-forced ENSO (Yuan et al., 2013).

The lag correlation analysis by Yuan et al. (2013) was limited by the short time series of the in situ and satellite observations since the 1990s. However, many studies have suggested a decadal variability of ENSO (Gershunov and Barnett, 1998; Wang and Picaut, 2004; An et al., 2005; Leloup et al., 2007) and/or IOD (Ashok et al., 2004; Abram et al., 2008; Ummenhofer et al., 2011) characteristics, as well as their interactions (Yuan and Li, 2008; Xie et al., 2010; Huang et al., 2010; Chowdary et al., 2012; Tao et al., 2014). The lag correlation between STIO SSTA in fall and Niño 3.4 SSTA in the following fall has been shown to be subjected to decadal variations in both observations and in historical simulations of the coupled climate models of the phase five Coupled Model Intercomparison Project (CMIP5) (Xu et al., 2013, manuscript). The results have also suggested that the oceanic channel dynamics of the IOD-forced ENSO are robust during positive phases (positive lag correlations between STIO SSTA in fall and Niño 3.4 SSTA in the following fall) in observations and in the CMIP5 climate coupled models. In this paper, we focus on the IOD-ENSO lag teleconnection during negative phases (negative lag correlations between STIO SSTA in fall and Niño 3.4 SSTA in the following fall) using observational SST data and Simple Ocean Data Assimilation (SODA) data to identify differences in the teleconnection between negative and positive phases.

The remainder of the paper is organized as follows. The next section introduces the data and methodology. In Section 3, the lag correlation between the IOD and ENSO during negative phases in SODA and related oceanic channel dynamics are described. A summary and conclusions are presented in Section 4.

2 DATA AND METHOD

2.1 Data description

The observational SST data used in this study are the Hadley Center sea ice and SST dataset (HadISST 1.1), the extended reconstruction of global SST dataset (ERSST V3b), and the Kaplan SST (Version 2.0) dataset. The HadISST covers the period from 1871 to the present with a resolution of 1°×1° based on in situ and satellite observations (Rayner et al., 2003). The ERSST is gridded from in situ SST data through empirical orthogonal function (EOF) projection, which allows stable reconstruction from sparse data. The dataset covers the period from January 1854 to the present on a 2°×2° horizontal grid (Smith et al., 2008). The Kaplan SST anomalies are derived from the United Kingdom Meteorology Office SST data using sophisticated statistical techniques to fill in the missing data (Kaplan et al., 1998). The dataset is stored on a 5°×5° grid and consists of monthly mean anomalies from 1856 to the present.

Version 2.2.4 of the SODA dataset is used to provide long time series of oceanic variables absent in the observational data. The SODA system is based on the Parallel Ocean Program model with an average resolution of 0.25°×0.4° at 40 vertical levels and covers the period of 1871–2010. The observational data in the SODA include virtually all available hydrographic profiles, ocean station data, moored

temperature and salinity time series, surface temperature and salinity, and nighttime infrared satellite SST data. The monthly mean output is remapped on a 0.5°×0.5° horizontal grid at 40 vertical levels (Carton and Giese, 2008).

2.2 Index definitions and statistical analysis

The Niño 3.4 index is defined as the average SSTA in the area of the equatorial central and eastern Pacific (5°S–5°N, 170°–120°W). The Dipole Mode Index (DMI) is calculated as the difference in SSTA between the western (10°S–10°N, 50°–70°E) and southeastern tropical Indian Ocean (10°S–0°, 90°–110°E) (Saji et al., 1999). The far western equatorial Pacific SZWA is averaged over 5°S–5°N, 130°–150°E.

The boreal seasons are defined as spring (March–May), summer (June–August), fall (September–November), and winter (December to the following February). Lag correlations are calculated using seasonal averaged anomalies. Student's *t*-test is used to evaluate the 95% significance level. Throughout this paper, the IOD year is referred to as Year 1, and the following year is referred to as Year 2.

3 IOD-ENSO TELECONNECTION DURING NEGATIVE PHASES IN THE SODA

3.1 Decadal variability of the IOD-ENSO teleconnection

The running mean lag correlation between the DMI in fall and the Niño 3.4 SSTA in the following fall, with a running window of 11 years, shows decadal variability in the SODA (solid thick line in Fig.1a), which is similar in the HadISST, ERSST, and Kaplan SST datasets (thin lines in Fig.1a). The hypothesis is that IOD-forced ENSO through oceanic channel dynamics (i.e., ITF variability) is started from the STIO (Yuan et al., 2011, 2013). Therefore, we use the running mean lag correlation between the STIO SSTA in fall and the Niño 3.4 SSTA in the following fall to identify the decadal variability of the IOD-ENSO teleconnection with a one-year time lag (Fig.1b). The results show that the running mean lag correlation of STIO SSTA suggests similar decadal variability in comparison with the DMI (Fig.1a, b). This decadal variability is supported by the 11-year running lag correlation of the SODA SSHA between the STIO and the central-eastern Pacific (Fig.1c). The results suggest that the lag correlation between the STIO SSHA in fall and the Niño 3.4 SSHA in the following fall has been predominately positive in most periods over the past century. The typical periods of variability of SSTA and SSHA lag correlations are about 16–18 years (Fig.1d–f). Throughout this paper, we refer to decades with a positive 11-year running lag correlation as positive phases, and decades with a negative correlation as negative phases. The positive phases are 1881–1889, 1898–1908, 1918–1929, 1948–1969, 1977–1985, and 1988–2010. The negative phases are 1871–1880, 1890–1897, 1909–1917, 1930–1947, and 1970–1976. It should be noted that the running lag correlation values in Fig.1a are barely significant because of the short time window. Nevertheless, the lag correlation for each positive phase, identified by the running lag correlation, is above the 95% significance level. To clarify why the IOD-ENSO teleconnection with a one-year time lag disappears during negative phases, we reconstructed a positive and a negative case that consists of each positive and negative period, respectively. The lag correlations between the STIO or the western equatorial Pacific anomalies and the tropical Indo-Pacific anomalies in the following sections are calculated based on the reconstructed positive and negative time series. It should also be noted that lag correlations with different running windows (11 years, 13 years, and 17 years) suggest similar positive or negative phase decades (figures omitted), confirming that lag correlation analysis in the negative phase decades is robust.

Lag correlation analysis during positive phases (right panels in Figs.3–5) shows that positive correlations above the 95% significance level move eastward from the STIO to the equatorial central and eastern Pacific cold tongue, which is consistent with the observations of Yuan et al. (2013). These results show that the oceanic channel dynamic, i.e., the ITF variability, plays an important role in connecting IOD forcing with the equatorial Pacific Ocean during positive phases. In the next section, we focus only on lag correlations during negative phases.

3.2 Oceanic channel dynamics

There are six typical El Niño (1877–78, 1896–97, 1911–12, 1913–14, 1930–31, 1972–73) and five La Niña events (1897–98, 1909–10, 1916–17, 1933–34, 1973–74), and nine typical positive IOD (1875–76, 1877–78, 1891–92, 1913–14, 1935–36, 1940–41, 1945–46, 1972–73) and nine negative IOD (1892–93, 1893–94, 1909–10, 1910–11, 1916–17, 1933–34, 1938–39, 1947–48, 1975–76) events in the negative phases identified by the SODA dataset. The Niño 3.4

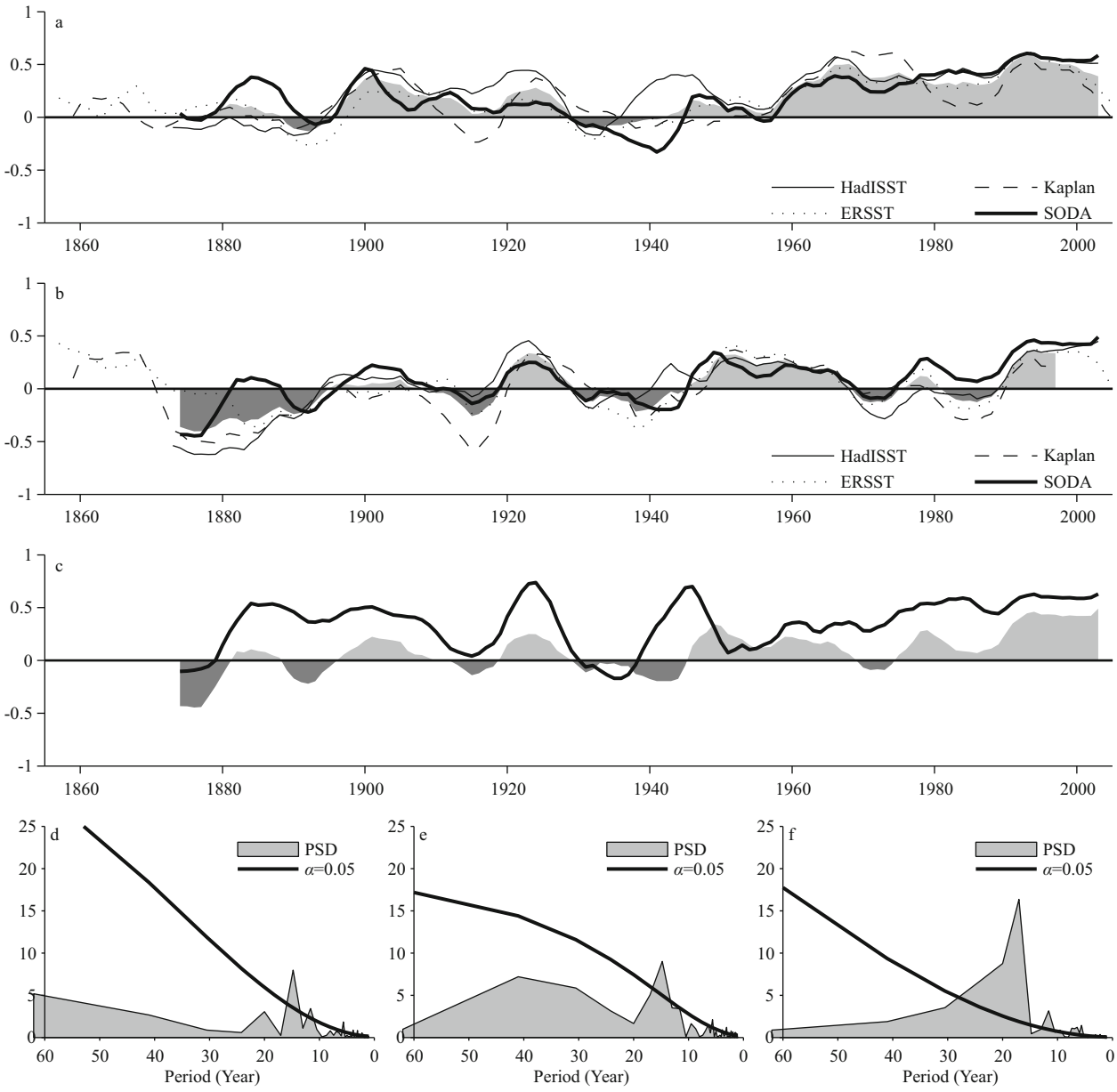

Fig.1 Decadal variability of the IOD-ENSO lag teleconnection

a. lag correlation between the DMI (the DMI has been multiplied by -1) in fall and the Niño 3.4 SSTA in the following fall with a running window of 11 years in observations; b. lag correlation between the STIO SSTA in fall and the Niño 3.4 SSTA in the following fall with a running window of 11 years in observations; c. l lag correlation between the SSTA (shading) or SSHA (solid line) in the STIO in fall and the Niño 3.4 area in the following fall with a running window of 11 years in the SODA. Power spectrum analysis of running mean lag correlation between (d) the DMI in fall and the Niño 3.4 SSTA in the following fall in the SODA; e. the STIO SSTA in fall and the Niño 3.4 SSTA in the following fall in the SODA; f. the STIO SSHA in fall and the Niño 3.4 SSHA in the following fall in the SODA. The shading in (a) and (b) indicates averages of the four datasets. The horizontal axes in (a) and (b) show the central date of the running window.

index and DMI in the SODA during negative phases are shown in Fig.2a and b, respectively. The ENSO events peak in the boreal winter (December to the following February), with maximum absolute values of about 3°C (Fig.2a). The IOD events are much weaker than the ENSO events, and peak in the boreal fall (September–November) with a maximum anomaly of only about 1°C (Fig.2b). Power spectrum analysis of the Niño 3.4 index and the DMI suggests a typical period for the ENSO cycle of 3–5 years (Fig.2c) and a quasi-biennial cycle for the IOD (Fig.2d). Regression analysis shows positive coefficients above the 95% significance level in the western tropical Indian Ocean and eastern equatorial Pacific Ocean, but negative coefficients above the 95% significance level in the STIO and western

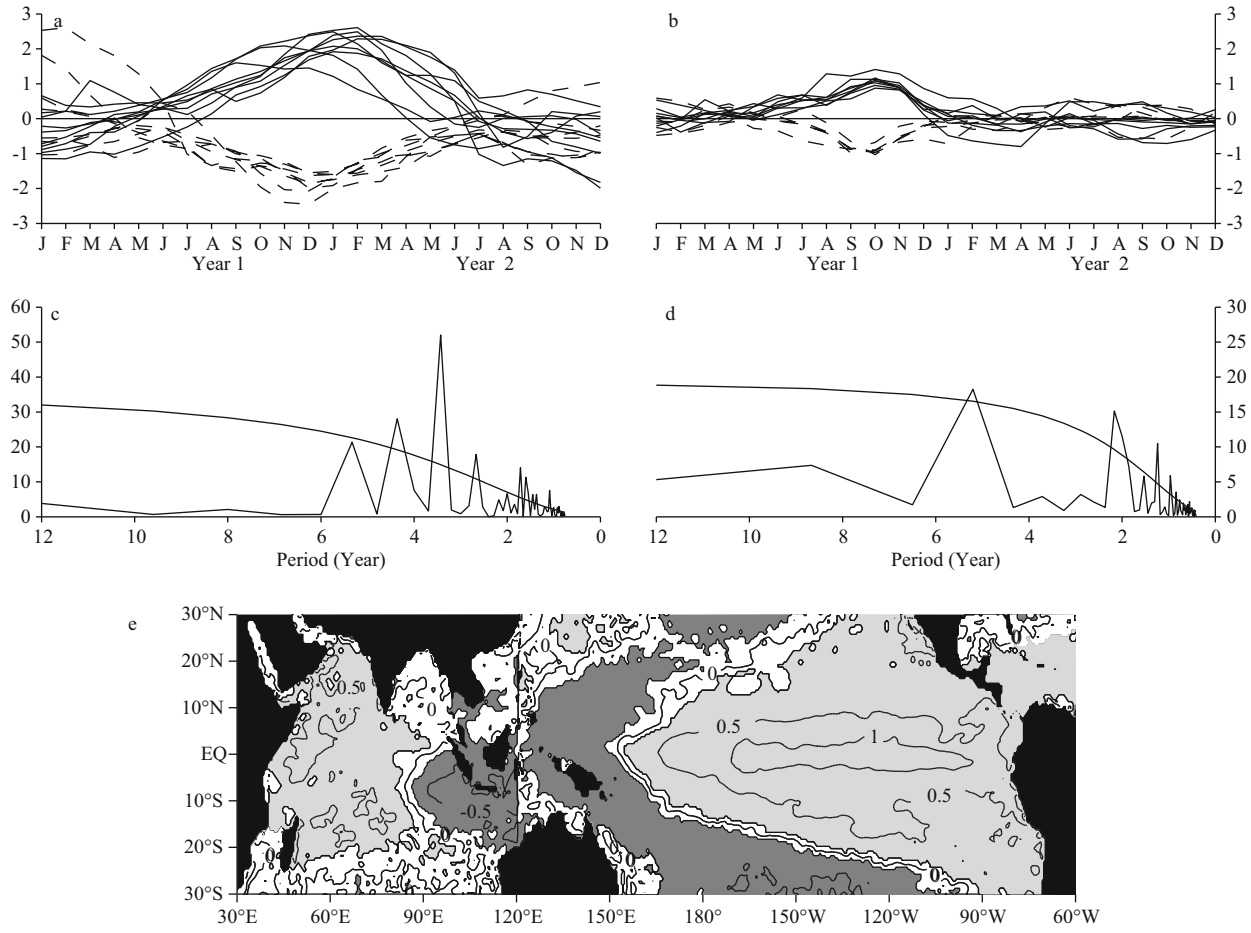

Fig.2 Characters of the IOD- and ENSO-type teleconnection

a. Niño 3.4 indices for each ENSO event during negative phases of the IOD-ENSO lag teleconnection; b. DMI for each IOD event during negative phases of the IOD-ENSO lag teleconnection. The solid (dashed) thin lines in (a) and (b) indicate El Niño (La Niña) and positive (negative) IOD events, respectively. The solid (dashed) thick lines in (a) and (b) are averaged from the thin lines; c. power spectrum analysis of the DMI during negative phases; d. power spectrum analysis of the Niño 3.4 index during negative phases. The thin lines in (c) and (d) indicate the 95% significance level; e. regression coefficients of SSTA on the DMI (in the Indian Ocean) and on the Niño 3.4 index (in the Pacific Ocean), light and dark shades indicate the 95% significance level of positive and negative coefficients, respectively.

equatorial Pacific Ocean. This suggests the same typical IOD- and ENSO-type teleconnection exists over the tropical Indo-Pacific Oceans during the negative phase as in the positive phase (Fig.2e).

Lag correlations between the STIO SSTA in fall and the tropical Indo-Pacific SSTA in the winter of Year 1 show significant IOD- and ENSO-type teleconnection, with negative correlations above the 95% significance level in the western tropical Indian Ocean and the eastern equatorial Pacific Ocean, and positive correlations in the western tropical Pacific Ocean (left panel of Fig.3a). The significant correlations in the equatorial Pacific cold tongue diminish in the spring of Year 2 and do not recur throughout Year 2 (left panels of Fig.3b–d), suggesting that the IOD-induced SSTA anomalies in the STIO are not precursors of ENSO predictability with a one-year time lag during negative phases of decadal variability. Lag correlations during positive phases, presented in the right panels in Fig.3 for comparison, show significant lag correlation in the cold tongue with a one-year time lag, suggesting enhanced predictability of ENSO provided by the IOD anomalies.

Lag correlations between the SSHA in the STIO in fall and in the tropical Indo-Pacific in the winter of Year 1 also show the same significant IOD- and ENSO-type teleconnection during the peak of the events, which is in agreement with the findings for the SSTA (left panel of Fig.4a). Positive correlations above the 95% significance level show eastward movement from the STIO to the equatorial Pacific Ocean through the Indonesian seas during Year 2 (Fig.4b–d). In the fall of Year 2, there are significant positive correlations in the equatorial Pacific cold

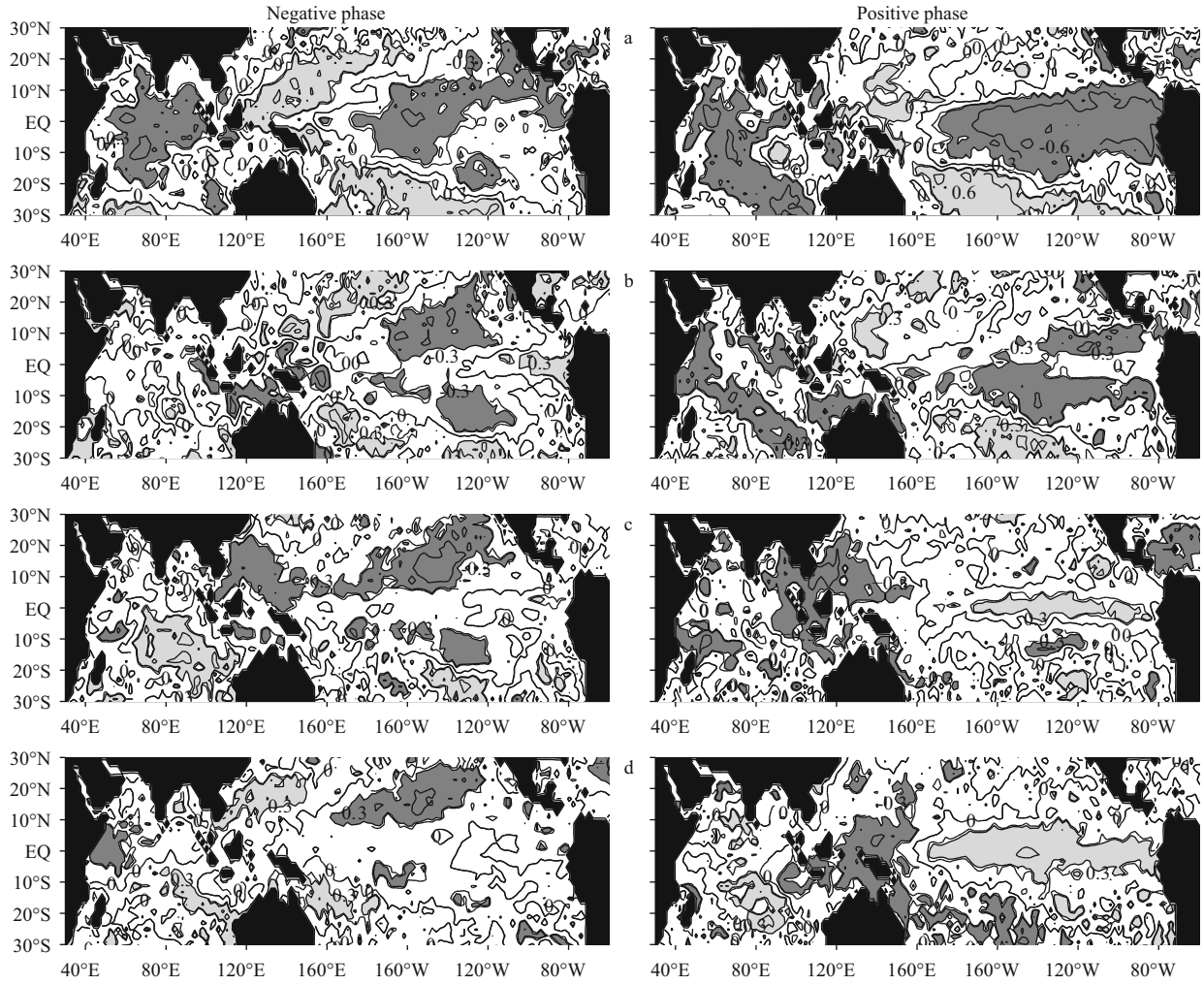

Fig.3 Lag correlations between the SSTA in the STIO in fall and in the tropical Indo-Pacific in the following winter through fall seasons

a. winter of Year 1 (December to the following February); b. spring of Year 2 (March–May); c. summer of Year 2 (June–August); d. fall of Year 2 (September–November). The contour interval is 0.3. Light and dark shades indicate the 95% significance level of positive and negative correlations, respectively.

tongue (Fig.4d). This process indicates that the SSHA in the STIO forces the ITF to transport more/less upper water from the Pacific Ocean to the Indian Ocean inducing thermocline anomalies in the equatorial western Pacific. The western Pacific thermocline anomalies propagate eastward as equatorial Kelvin waves, favoring cold tongue cooling/warming with a one-year time lag. This oceanic channel dynamic in the negative phase is as important as in the positive phase in connecting the IOD forcing on ENSO with a one-year time lag. However, insignificant lag correlations between the STIO SSTA in fall and the cold tongue SSTA in the fall of Year 2 (left panel of Fig.3d) suggest that the oceanic channel dynamics are not responsible for the equatorial Pacific cold tongue warming or cooling with a one-year time lag.

The significant ENSO-type teleconnection in the winter of Year 1 is also suggested by the lag correlations of subsurface temperature anomalies. Lag correlations between the STIO SSTA in the fall of Year 1 and the temperature anomalies in the vertical section of the equatorial Pacific in the winter of Year 2 show negative and positive correlations above the 95% significance level in the western and eastern Pacific, respectively. The significant negative correlations diminish in the spring of Year 2 in the upper layer of the equatorial Pacific Ocean. The eastward propagation of positive correlations of subsurface temperature anomalies in the vertical section of the equatorial Pacific Ocean is evidenced by the eastward extension of the zero contours in the right panels of Fig.5. However, the significant positive correlations in the subsurface of the equatorial Pacific

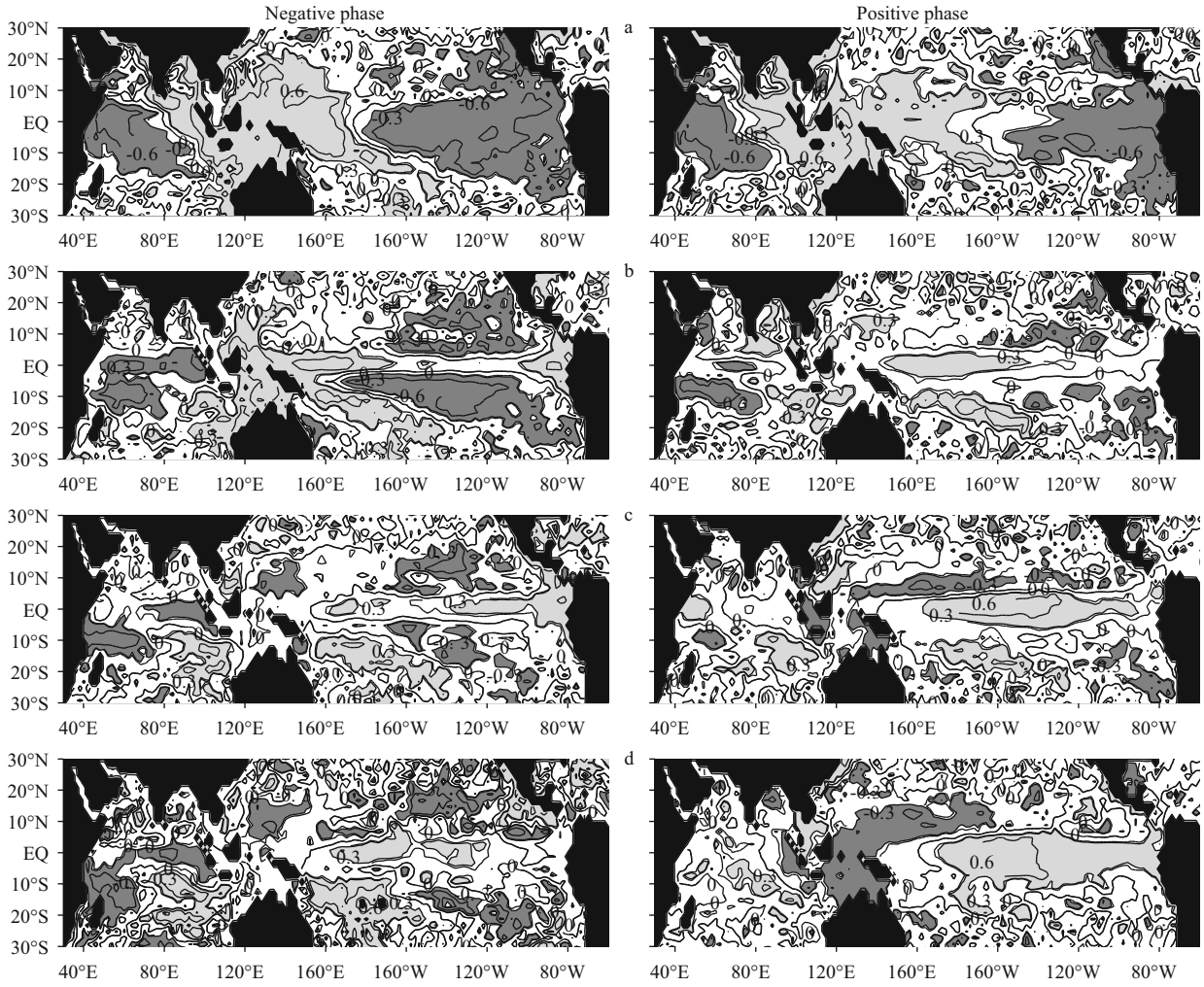

Fig.4 Lag correlations between the SSHA in the STIO in fall and the tropical Indo-Pacific SSHA in the following winter through fall seasons

a. winter of Year 1 (December to the following February); b. spring of Year 2 (March–May); c. summer of Year 2 (June–August); d. fall of Year 2 (September–November). The contour interval is 0.3. Light and dark shades indicate the 95% significance level of positive and negative correlations, respectively.

stay at much greater depths than during positive phases (Fig.5). In addition, the significant positive correlations do not outcrop in the equatorial Pacific cold tongue in the summer and fall seasons of Year 2. These results explain the insignificant correlation between the STIO SSTA in fall and the SSTA in the cold tongue with a one-year time lag.

3.3 Role of the atmospheric bridge

Izumo et al. (2010) suggested that the atmospheric bridge plays an important role in carrying the IOD signal to the western equatorial Pacific Ocean to influence the cold tongue SSTA one year later. Based on lag correlation analysis, Yuan et al. (2013) argued that the lag correlations between the SZWA over the far western equatorial Pacific in the fall of Year 1 and the Indo-Pacific SZWA, SSTA, and SSHA in the equatorial Pacific cold tongue in fall of Year 2 are all insignificant. Therefore, the enhanced predictability of ENSO with a one-year time lag should not be attributed to the atmospheric bridge.

In the present study, a similar correlation analysis is conducted to identify any relationship between IOD and ENSO through the atmospheric bridge process during negative phases. The correlations between SZWA over the far western equatorial Pacific in fall and the Pacific SSTA/SSHA in the following fall show correlations above the 95% significance level only in the west equatorial Pacific or off-equatorial Pacific Ocean (Fig.6). These results suggest that atmospheric bridge processes are not responsible for the equatorial Pacific cold tongue warming/cooling with a one-year time lag during negative phases because of the short lived atmospheric signals.

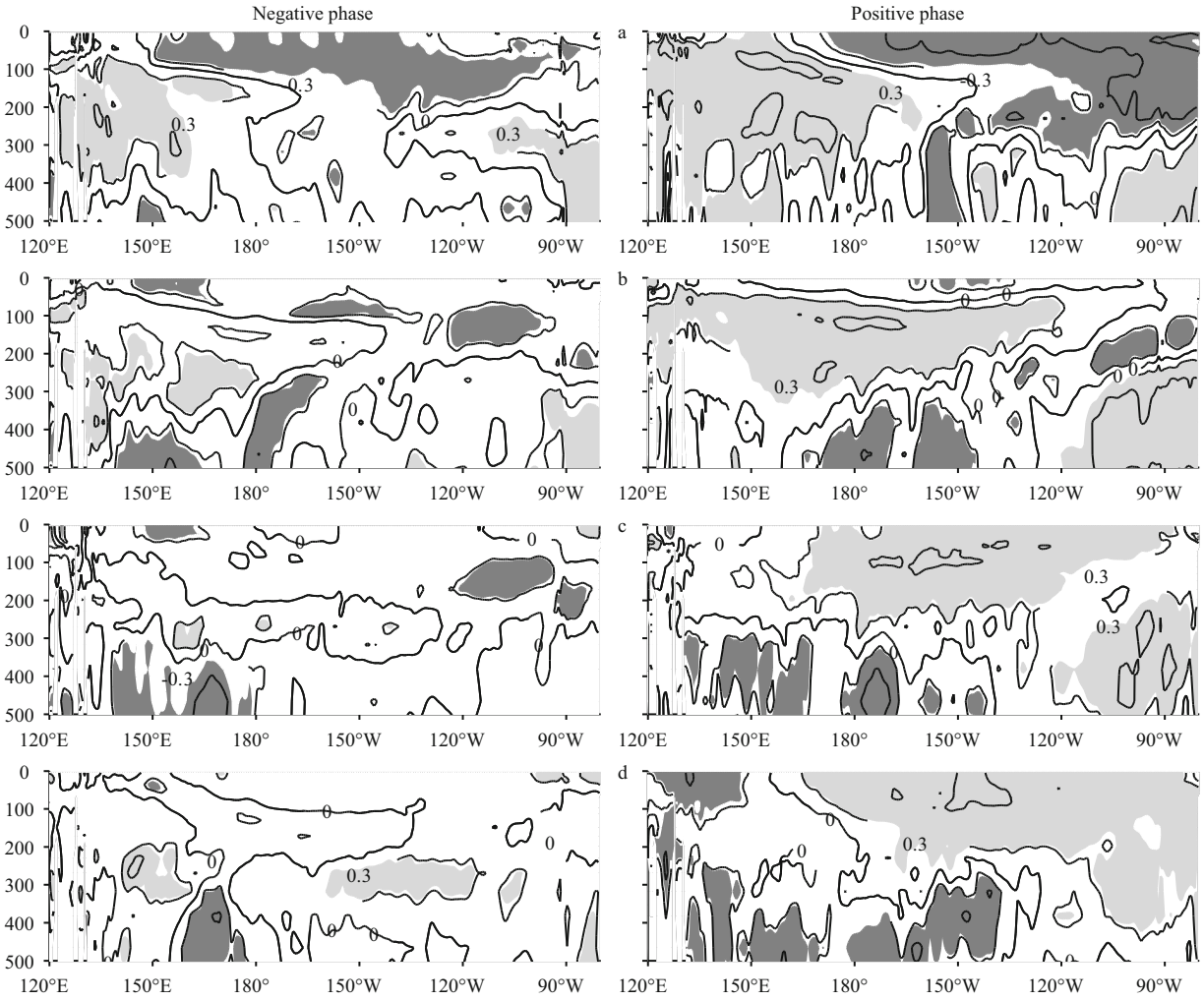

Fig.5 Lag correlations between the SSTA in the STIO in fall and the temperature anomalies along the vertical section of the equatorial Pacific in the following winter through fall seasons

a. winter of Year 1 (December to the following February); b. spring of Year 2 (March–May); c. summer of Year 2 (June–August); d. fall of Year 2 (September–November). The contour interval is 0.3. Light and dark shades indicate the 95% significance level of positive and negative correlations, respectively.

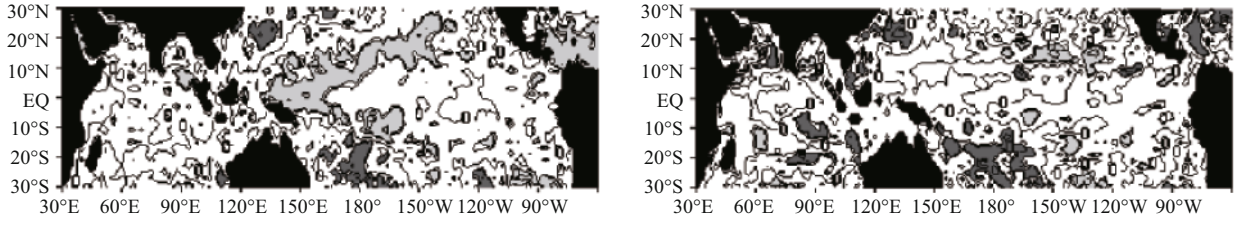

Fig.6 Lag correlations between the SZWA over the far western equatorial Pacific in fall and the tropical Indo-Pacific oceanic anomalies in the following fall

a. lag correlations between the SZWA over the far western equatorial Pacific in fall and the tropical Indo-Pacific SSTA in the following fall; b. lag correlations between the SZWA over the far western equatorial Pacific in fall and the tropical Indo-Pacific SSHA in the following fall. The contour interval is 0.3. Light and dark shades indicate the 95% significance level of positive and negative correlations, respectively.

3.4 Role of the west Pacific warm pool

The SSTA in the equatorial Pacific cold tongue in the fall of Year 2 do not arise from the SSTA in the west Pacific warm pool (WPWP) in fall of Year 1 during positive phases (Yuan et al., 2013). However, during negative phases, the cold tongue SSTA in fall are closely related to WPWP SSTA in the previous fall. Lag correlations between the WPWP SSTA in fall and the Indo-Pacific SSTA in the winter of Year 1 show negative correlations above the 95% significance level in the eastern tropical Pacific Ocean, juxtaposing

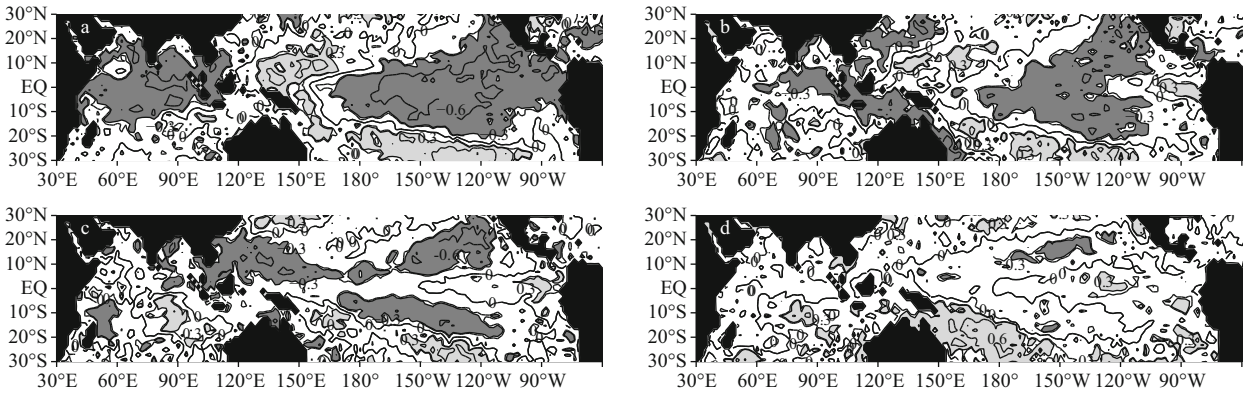

Fig.7 Lag correlations between the SSTA in the western equatorial Pacific Ocean in fall and the tropical Indo-Pacific SSTA in the following winter through fall seasons

a. winter of Year 1 (December to the following February); b. spring of Year 2 (March–May); c. summer of Year 2 (June–August); d. fall of Year 2 (September–November). The contour interval is 0.3. Light and dark shades indicate the 95% significance level of positive and negative correlations, respectively.

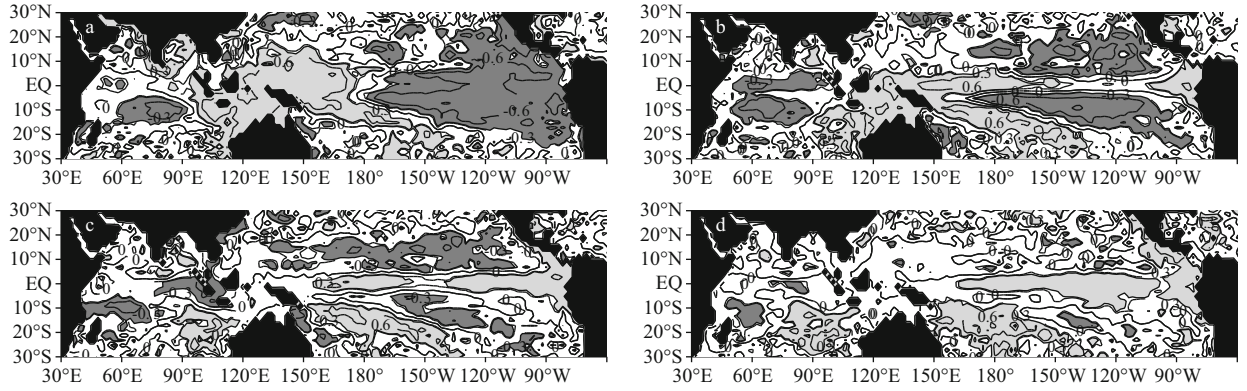

Fig.8 Lag correlations between the SSHA in the western equatorial Pacific Ocean in fall and the tropical Indo-Pacific SSHA in the following winter through fall seasons

a. winter of Year 1 (December to the following February); b. spring of Year 2 (March–May); c. summer of Year 2 (June–August); d. fall of Year 2 (September–November). The contour interval is 0.3. Light and dark shades indicate the 95% significance level of positive and negative correlation, respectively.

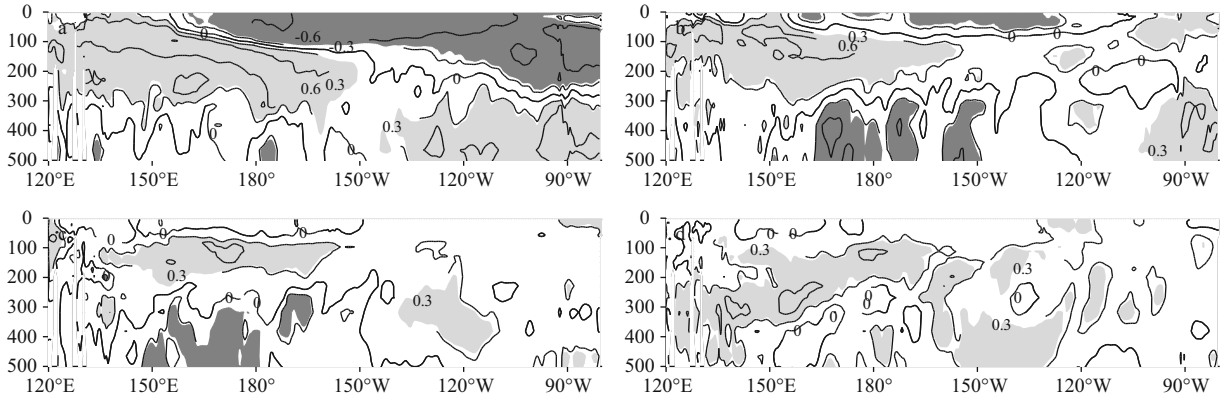

Fig.9 Lag correlations between the SSTA in the western equatorial Pacific Ocean in fall and the temperature anomalies along the equatorial Pacific vertical section in the following winter through fall seasons

a. winter of Year 1 (December to the following February); b. spring of Year 2 (March–May); c. summer of Year 2 (June–August); d. fall of Year 2 (September–November). The contour interval is 0.3. Light and dark shades indicate the 95% significance level of positive and negative correlation, respectively.

with significant positive correlations in the west and off-equatorial Pacific Ocean (Fig.7a). The significant negative correlations diminish in spring of Year 2. Significant positive lag correlations develop in the eastern and central equatorial Pacific Ocean in the summer and fall of Year 2 (Fig.7c, d), suggesting that the SSTA in fall of Year 2 are statistically associated with the WPWP SSTA in the previous fall (Fig.7d).

The impact of the WPWP anomalies on the anomalies in the central and eastern equatorial Pacific cold tongue is supported by the lag correlations between the WPWP SSHA in fall and the SSHA in the Indo-Pacific Oceans in the following winter through fall seasons. There are significant IOD- and ENSO-type teleconnections, with a negative-positive-negative distribution of lag correlations above the 95% significance level over the Indo-Pacific basin in the winter of Year 1 (Fig.8a). Throughout spring to fall of Year 2, there is an eastward movement of positive correlations above the 95% significance level from the western equatorial Pacific to the east, suggesting eastward propagation of equatorial Kelvin waves derived from the western equatorial Pacific (Fig.8b–d).

The significant correlation between the WPWP SSTA in fall and the SSTA in the central and eastern equatorial Pacific Ocean with a one-year time lag is further explained by the lag correlations of subsurface temperature anomalies. The correlations between the WPWP SSTA in fall and temperature anomalies in the vertical section of the equatorial Pacific in the following winter are positive above the 95% significance level in the west and negative in the east (Fig.9a), in agreement with the correlations of SSTA and SSHA. The significant positive correlations propagate eastward in the subsurface in Year 2 (Fig.9b–d). The significant positive correlations surface in the equatorial Pacific cold tongue (Fig.9d), which explains the significant correlations between the WPWP SSTA in fall and the SSTA in the cold tongue with a one-year time lag.

The above analysis suggests significant teleconnection between the WPWP and the equatorial Pacific cold tongue with a one-year time lag during negative phases. However, this teleconnection during positive phases was not significant, because the correlations between the WPWP SSTA/SSHA in fall and the cold tongue SSTA/SSHA in the following fall were not significant (Yuan et al., 2013). The teleconnection between IOD and ENSO with a one-year time lag is probably depressed by the ENSO modulation in the Pacific Ocean during negative phases.

4 SUMMARY

Lag correlation analysis of observational data since 1990 has shown significant IOD-ENSO teleconnection with a one-year time lag through oceanic channel dynamics (Yuan et al., 2013). The IOD-ENSO teleconnection with a one-year time lag is subject to decadal variations, showing negative, albeit insignificant, lag correlations between the STIO SSTA in fall and SSTA in the cold tongue with a one-year time lag during some decades. However, lag correlations between the STIO SSHA in fall and the SSHA in the cold tongue with a one-year time lag were positive above the 95% significance level. The lag correlations between the STIO SSTA in fall and the equatorial Pacific subsurface temperature anomalies have shown evidence of eastward propagation in the vertical section of the equatorial Pacific. However, the eastward propagating correlations in the subsurface were below the 95% significance level and at much greater depths. These results indicate that oceanic channel dynamics are not able to predict cold tongue SSTA with a one-year time lag.

Significant lag correlations between the SZWA over the far western Pacific in fall and the Indo-Pacific SSTA/SSHA were insignificant in the following fall, suggesting that the atmospheric signals were short lived and were not able to explain the negative teleconnection between IOD and ENSO. Conversely, lag correlations between the WPWP SSTA/SSHA in fall and the Indo-Pacific SSTA/SSHA in the cold tongue were positive above the 95% significance level with a one-year time lag. Further investigation of correlations of subsurface temperature anomalies indicated that the anomalies in the western equatorial Pacific in the fall of Year 1 were propagating eastward in the subsurface in Year 2. The anomalies surfaced in the central and eastern equatorial Pacific in the fall of Year 2 to induce cold tongue warming/cooling. This process was much stronger and at a shallower depth than the anomalies induced by oceanic channel dynamics, suggesting that oceanic channel dynamics carrying SSTA from the STIO to the equatorial Pacific were overwhelmed by the stronger coupling processes related to the ENSO over the WPWP.

References

Abram N J, Gagan M K, Cole J E, Hantoro W S, Mudelsee M. 2008. Recent intensification of tropical climate variability in the Indian Ocean. *Nat. Geosci*., **1**: 849-853.

Alexander M A, Bladé I, Newman M, Lanzante J R, Lau N C, Scot J D. 2002. The atmospheric bridge: the influence of ENSO teleconnections on air-sea interaction over the global oceans. *J. Climate*, **15**: 2 205-2 231.

An S I, Hsieh W W, Jin F F. 2005. A nonlinear analysis of the ENSO cycle and its interdecadal changes. *J. Climate*, **18**: 3 229-3 239

Annamalai H, Xie S P, McCreary J P, Murtugudde R. 2005. Impact of Indian Ocean sea surface temperature on developing El Niño. *J. Climate*, **18**: 302-319.

Ashok K, Chan W L, Motoi T, Yamagata T. 2004. Decadal

variability of the Indian Ocean Dipole. *Geophys*. *Res*. *Lett*., **31**: L24207, http://dx.doi.org/10.1029/2004GL021345.

Behera S K, Luo J J, Masson S, Rao S A, Sakuma H, Yamagata T. 2006. A CGCM study on the interaction between IOD and ENSO. *J*. *Climate*, **19**: 1 688-1 705.

Cai W J, Meyers G, Shi G. 2005. Transmission of ENSO signal to the Indian Ocean. *Geophys*. *Res*. *Lett*., **32**: L05616, http://dx.doi.org/10.1029/2004GL021736.

Carton J A, Giese B S. 2008. A reanalysis of ocean climate using simple ocean data assimilation (SODA). *Monthly Weather Review*, **136**: 2 999-3 017.

Chowdary J S, Xie S P, Tokinaga H, Okumura Y M, Kubota H, Johnson N C, Zheng X T. 2012. Interdecadal variations in ENSO teleconnection to the Indo-western Pacific for 1870-2007. *J*. *Climate*, **25**: 1 722-1 744.

Dominiak S, Terray P. 2005. Improvement of ENSO prediction using a linear regression model with a southern Indian Ocean sea surface temperature predictor. *Geophys*. *Res*. *Lett*.,**32**:L18702,http://dx.doi.org/10.1029/2005GL023153.

Du Y, Xie S P, Hu K, Huang G. 2009. Role of air-sea interaction in the long persistence of El Niño-induced north Indian Ocean warming. *J*. *Climate*, **22**: 2 023-2 038.

Gershunov A, Barnett T. 1998. Interdecadal modulation of ENSO teleconnection. *Bull*. *Amer*. *Meteor*. *Soc*., **79**: 2 715-2 725.

Huang G, Hu K M, Xie S P. 2010. Strengthening of tropical Indian Ocean teleconnection to the northwest Pacific since the Mid-1970s: an atmospheric GCM study. *J*. *Climate*, **23**: 5 294-5 304.

Izumo T, Legaigne M, Vialard J, Luo J J, Yamagata T, Madec G. 2013. Influence of the Indian Ocean Dipole and Pacific recharge on following year's El Niño: interdecadal robustness. *Clim*. *Dynam*., http://dx.doi.org/10.1007/s00382-012-1628-1.

Izumo T, Vialard J, Lengaigne M, Clement de B M, Behera S K, Luo J J, Cravatte S, Masson S, Yamagata T. 2010. Influence of the Indian Ocean Dipole on following year's El Niño. *Nat*. *Geosci*., **3**: 168-172.

Kaplan A, Cane M, Kushnir Y et al. 1998. Analyses of global sea surface temperature 1856-1991. *J*. *Geophy*. *Res*., **103**: 567-589.

Klein S A, Soden B J, Lau N C. 1999. Remote sea surface temperature variations during ENSO: evidence for a tropical atmospheric bridge. *J*. *Climate*, **12**: 917-932.

Kug J S, Ham Y G. 2012. Indian Ocean feedback to the ENSO transition in a multi-model ensemble. *J*. *Clim*., **25**: 6 942-6 957.

Lau N C, Nath M J. 2003. Atmosphere-ocean variations in the Indo-Pacific sector during ENSO episodes. *J*. *Climate*, **16**: 3-20.

Leloup J A, Lachkar Z, Boulanger J P, Thiria S. 2007. Detecting decadal changes in ENSO using neural networks. *Clim*. *Dyn*., http://dx.doi.org/10.1007/s00382-006-0173-13.

Luo J J, Zhang R, Behera S, Masumoto Y, Jin F F, Lukas R, Yamagata T. 2010. Interaction between El Niño and extreme Indian Ocean Dipole. *J*. *Climate*, **23**: 726-742.

Ohba M, Nohara D, Ueda H. 2010. Simulation of asymmetric ENSO transition in WCRP CMIP3 multi-model experiments. *J*. *Climate*, http://dx.doi.org/10.1175/2010JCLI3608.1.

Okumura Y M, Deser C. 2010. Asymmetry in the duration of El Niño and La Niña. *J*. *Climate*, **23**: 5 826-5 843.

Rayner N A, Parker D E, Horton E B, Folland C K, Alexander L V, Rowell D P, Kent E C, Kaplan A. 2003. Global analyses of sea surface temperature, sea ice, and night marine air temperature since the late nineteenth century. *J*. *Geophys*. *Res*., **108**: 4 407, http://dx.doi.org/10.1029/2002JD002670.

Saji N H, Goswami B N, Vinayachandran P N, Yamagata T. 1999. A dipole mode in the tropical Indian Ocean. *Nature*, **401**: 360-363.

Santoso A, England M H, Cai W. 2012. Impact of Indo-Pacific feedback interactions on ENSO dynamics diagnosed using ensemble climate simulations. *J*. *Climate*, **25**: 7 743-7 763.

Smith T M, Reynolds R W, Peterson T C, Lawrimore J. 2008. Improvement to NOAA's historical merged Land-Ocean surface temperature analysis (1880-2006). *J*. *Climate*, **21**: 2 283-2 296.

Tao W C, Huang G, Hu K M, Qu X, Wen G H, Gong H N. 2014. Interdecadal modulation of ENSO teleconnections to the Indian Ocean Basin Mode and their relationship under global warming in CMIP5 models. *International Journal of Climatology*, http://dx.doi.org/10.1002/joc.3987.

Ummenhofer C C, Sen Gupta A, Li Y, Taschetto A S, England M H. 2011. Multi-decadal modulation of the El Niño-Indian monsoon relationship by Indian Ocean variability. *Environ*. *Res*. *Lett*., http://dx.doi.org/10.1088/1748-9326/6/3/034006.

Wang C, Picaut J. 2004. Understanding ENSO physics—a review. *In*: Wang C, Xie S-P, Carton J A eds. Earth's climate: the oceanatmosphere interaction. AGU Geophysical Monograph Series. **147**: 21-48.

Webster P J, Moore A M, Loschnigg J P, Leben R R. 1999. Coupled ocean-atmosphere dynamics in the Indian Ocean during 1997-1998. *Nature*, **401**: 356-360.

Wu R, Kirtman B P. 2004. Understanding the impacts of the Indian Ocean on ENSO variability in a coupled GCM. *J*. *Climate*, **17**: 4 019-4 031.

Xie S P, Du Y, Huang G, Zheng X T, Tokinaga H, Hu K M, Liu Q Y. 2010. Decadal shift in El Niño influences on Indo-Western Pacific and East Asian Climate in the 1970s. *J*. *Climate*, **23**: 3 352-3 368.

Xie S P, Hu K, Hafner J, Tokinaga H, Du Y, Huang G, Sampe T. 2009. Indian Ocean capacitor effect on Indo-western Pacific climate during the summer following El Niño. *J*. *Climate*, **22**: 730-747.

Yuan D L, Wang J, Xu T F, Xu P, Zhou H, Zhao X, Luan Y H, Zheng W P, Yu Y Q. 2011. Forcing of the Indian Ocean dipole on the interannual variations of the Tropical Pacific Ocean: Roles of the Indonesian throughflow. *J*. *Climate*, **15**: 3 597-3 608.

Yuan D L, Zhou H, Zhao X. 2013. Interannual climate variability over the tropical Pacific Ocean induced by the Indian Ocean dipole through the Indonesian Throughflow. *J*. *Climate*, **26**: 2 845-2 861.

Yuan Y, Li C Y. 2008. Decadal variability of the IOD-ENSO relationship. *Chinese Science Bulletin*, **53**(11): 1 746-1 752.